doi:10.1093/brain/awz391 BRAIN 2020: 143; 441–451 | 441

BRAIN
A JOURNAL OF NEUROLOGY

REPORT

Homozygous *STXBP1* variant causes encephalopathy and gain-of-function in synaptic transmission

Hanna C.A. Lammertse,[1,2,*] Annemiek A. van Berkel,[1,2,*] Michele Iacomino,[3] Ruud F. Toonen,[2] Pasquale Striano,[4,5] Antonio Gambardella,[6] Matthijs Verhage[1,2] and Federico Zara[3]

*These authors contributed equally to this work.

Heterozygous mutations in the *STXBP1* gene encoding the presynaptic protein MUNC18-1 cause *STXBP1* encephalopathy, characterized by developmental delay, intellectual disability and epilepsy. Impaired mutant protein stability leading to reduced synaptic transmission is considered the main underlying pathogenetic mechanism. Here, we report the first two cases carrying a homozygous *STXBP1* mutation, where their heterozygous siblings and mother are asymptomatic. Both cases were diagnosed with Lennox-Gastaut syndrome. In Munc18-1 null mouse neurons, protein stability of the disease variant (L446F) is less dramatically affected than previously observed for heterozygous disease mutants. Neurons expressing Munc18^{L446F} showed minor changes in morphology and synapse density. However, patch clamp recordings demonstrated that L446F causes a 2-fold increase in evoked synaptic transmission. Conversely, paired pulse plasticity was reduced and recovery after stimulus trains also. Spontaneous release frequency and amplitude, the readily releasable vesicle pool and the kinetics of short-term plasticity were all normal. Hence, the homozygous L446F mutation causes a gain-of-function phenotype regarding release probability and synaptic transmission while having less impact on protein levels than previously reported (heterozygous) mutations. These data show that *STXBP1* mutations produce divergent cellular effects, resulting in different clinical features, while sharing the overarching encephalopathic phenotype (developmental delay, intellectual disability and epilepsy).

1 Department of Clinical Genetics, Center for Neurogenomics and Cognitive Research (CNCR), University Medical Center Amsterdam, De Boelelaan 1085, 1081 HV Amsterdam, The Netherlands
2 Department of Functional Genomics, Center for Neurogenomics and Cognitive Research (CNCR), VU University Amsterdam, De Boelelaan 1085, 1081 HV Amsterdam, The Netherlands
3 Laboratory of Neurogenetics and Neuroscience, IRCCS Istituto G. Gaslini, Via Gerolamo Gaslini 5, 16147 Genova, Italy
4 IRCCS Istituto "G. Gaslini", Genova, Italy
5 Department of Neurosciences, Rehabilitation, Ophthalmology, Genetics, Maternal and Child Health, University of Genova, Genova, Italy
6 Institute of Neurology, University Magna Græcia, Catanzaro, Italy

Correspondence to: M. Verhage
Department of Clinical Genetics, Center for Neurogenomics and Cognitive Research (CNCR), University Medical Center Amsterdam, De Boelelaan 1085, 1081 HV Amsterdam, The Netherlands
E-mail: matthijs@cncr.vu.nl

Correspondence may also be addressed to: A. Gambardella
Institute of Neurology, University Magna Græcia, Catanzaro, Italy
E-mail: a.gambardella@unicz.it

Received June 5, 2019. Revised October 9, 2019. Accepted October 29, 2019. Advance Access publication December 19, 2019

Keywords: *STXBP1*; epilepsy; neurodevelopmental disorder; Lennox-Gastaut syndrome; synaptic transmission

Abbreviations: EPSC = excitatory postsynaptic current; RRP = readily releasable pool

Introduction

Mutations in the *STXBP1* gene are associated with infantile encephalopathy (Saitsu *et al.*, 2008), recently termed '*STXBP1* encephalopathy' (Stamberger *et al.*, 2016). Developmental delay and intellectual disability are hallmarks of *STXBP1* encephalopathy. Most patients experience epileptic seizures (Hamdan *et al.*, 2011; Gburek-Augustat *et al.*, 2016). Clinical heterogeneity is observed for patients carrying a *STXBP1* mutation, such as the severity of the developmental delay and intellectual disability, response to antiepileptic treatment and specific EEG abnormalities. This clinical heterogeneity leads to range of clinical diagnoses, including Ohtahara, and West syndromes (Stamberger *et al.*, 2016).

The *STXBP1* gene encodes the Sec1p/Munc18 (SM) protein MUNC18-1. Mammalian MUNC18-1 organizes the protein complexes that drive secretory vesicle exocytosis (Toonen and Verhage, 2007). Synaptic transmission is critically dependent on MUNC18-1 (Verhage *et al.*, 2000) and cellular MUNC18-1 levels correlate with synaptic strength (Toonen *et al.*, 2006).

All currently reported patients with *STXBP1* encephalopathy carry a heterozygous mutation, ranging from full gene deletions to single point mutations occurring across the entire length of the gene (Stamberger *et al.*, 2016). Multiple lines of evidence support the hypothesis that haploinsufficiency is the main pathogenic mechanism underlying *STXBP1* encephalopathy, which may explain the lack of a genotype–phenotype correlation. The probability of being loss-of-function intolerant is extremely high for *STXBP1* (pLI = 1), and it is therefore considered to fall in the 'haploinsufficient' gene category (gnomAD v2.1) (Kovačević *et al.*, 2018; Karczewski *et al.*, 2019). *STXBP1* encephalopathy variants affect the cellular levels of the Munc18-1 protein in *in vitro* models of the disease (Saitsu *et al.*, 2010; Guiberson *et al.*, 2018; Kovačević *et al.*, 2018). Moreover, heterozygous *Stxbp1* (Munc18-1 null) mice recapitulate *STXBP1* encephalopathy symptoms including cognitive impairments and epileptic seizures (Kovačević *et al.*, 2018; Orock *et al.*, 2018).

Here, we present two siblings carrying a homozygous *STXBP1* mutation and displaying the electroclinical features of Lennox-Gastaut syndrome. The functional consequences of the mutation in a cellular model are strikingly different from heterozygous mutations modelled previously (Guiberson *et al.*, 2018; Kovačević *et al.*, 2018).

Materials and methods

Animals

Munc18-1 null mutant (knockout) mice were described previously (Verhage *et al.*, 2000). Embryonic Day 18 (E18) embryos were obtained by caesarean section. Animals were housed and bred according to the Institutional and Dutch governmental guidelines.

Primary neuronal cultures

Neuronal cultures and rat glia islands were prepared as described previously (Santos *et al.*, 2016; Kovačević *et al.*, 2018). Cortical neurons were plated at a density of 600 000 cells/well on poly-L-ornithine/laminin coated 6-well plates for western blot analysis. Hippocampal neurons were plated at a density of 6000 cells/well on top of pregrown rat glia islands on 18 mm coverslips for immunocytochemistry and electrophysiology.

Constructs and lentiviral particles

Constructs encoding pSynapsin-Munc18^{WT}-T2A-CreGFP or pSynapsin-Munc18^{L446F}-T2A-CreGFP were subcloned into pLenti vectors, and viral particles were produced as previously described (Naldini *et al.*, 1996; Kovačević *et al.*, 2018). Munc18-1 null neurons were infected with lentiviral particles at 0 days *in vitro* (DIV).

Western blot

HEK293T cells were infected with lentiviral particles expressing Munc18^{WT} or Munc18^{L446F} in Opti-MEM^{TM} (Life Technologies) for 2 days. Neuronal cultures were collected at DIV 14. Western blot was executed as described (Kovačević *et al.*, 2018). Protein levels were assessed using rabbit Munc18-1 (1:1000, 2701; Cijsouw *et al.*, 2014) and mouse GFP (1:1000, eBioscience). GFP and Munc18-1 are translated in a 1:1 ratio as a result of the T2A linking sequence. GFP levels were used to normalize Munc18-1 expression levels.

Immunocytochemistry and confocal microscopy

Single isolated Munc18-1 null neurons expressing Munc18^{WT} or Munc18^{L446F} were fixed on DIV 14–15 with 3.7% formaldehyde. Neurons were stained as described previously (Santos *et al.*, 2016). Antibodies used were chicken anti-MAP2 (1:500; Abcam), rabbit anti-Munc18-1 (1:500; 2701; Cijsouw *et al.*, 2014) and mouse anti-VAMP (1:1000; SySy). Images were acquired with a confocal microscope (LSM 510, Carl Zeiss) using a 40× oil immersion objective (NA = 1.3) with

0.7× zoom at 1024 × 1024 pixels and 2× averaging. Synapse morphology and protein levels were analysed using automated image analysis in MATLAB (SynD; Schmitz *et al.*, 2011) and ImageJ software.

Electrophysiology

Single isolated Munc18-1 null neurons were in culture for DIV 14–15 prior to patch-clamp recordings. Recordings were performed as described previously (Meijer *et al.*, 2015; Kovačević *et al.*, 2018) and the experimenter was blinded to experimental groups. Analysis was performed using in-house written MATLAB scripts and Clampfit (Molecular Devices, v. 10.7). Size of the readily releasable pool (RRP) and the recruitment rate were estimated by a back-extrapolation procedure (Supplementary Fig. 3A) (Neher, 2015).

Statistical analysis

Statistical analysis and graphing was performed using GraphPad Prism versions 5 and 6 and MATLAB (MathWorks Inc., v.2017a). Parametric tests were used whenever assumptions of homoscedasticity and normality were met. Otherwise, non-parametric tests were used. All statistical tests were two-tailed. An error probability level of $P < 0.05$ was accepted as statistically significant. All cellular data were plotted in box-and-whisker plots with Tukey-style whiskers.

Data availability

Data are available upon request.

Results

Only homozygous *STXBP1*^{L446F} carriers show developmental epileptic encephalopathy

A family with two siblings with epilepsy and intellectual disability referred to the Neurology Unit at University Magna Graecia. The first proband (Individual 2, Table 1) was a 23-year-old female, presenting with development delay from birth, refractory epilepsy, severe intellectual disability and behavioural abnormalities. Multiple seizure types were observed, including tonic, atypical absences, 'drop attacks' and occasional catamenial non-convulsive status epilepticus, lasting up to several hours. Awake and sleep EEG recordings revealed a slow, disorganized background activity and high voltage, generalized 1.5–2 cycles/s spike and wave activity in addition to bursts of 10–12 Hz generalized paroxysmal fast activity during slow sleep (Fig. 1B). The 26-year-old sister (Individual 3, Table 1) displayed a highly similar neurological and electroclinical phenotype, albeit with more moderate intellectual disability. Both probands are on anti-epileptic polytherapy, achieving partial seizure control in proband 3. Their 51-year-old mother, and their 28- and 20-year-old sisters were asymptomatic and showed normal intelligence.

Whole-exome sequencing in the probands revealed a homozygous missense variant in exon 15 (c.1336C>T, p.L446F) of *STXBP1* (Fig. 1C and Supplementary Fig. 1). The mother and one sibling were heterozygous carriers of the mutation (Fig. 1C). Protein sequence alignment showed that the Leu446 residue is evolutionary conserved from *Caenorhabditis elegans* to *Homo sapiens* (Fig. 1D). The L446F variant is located in domain 3 of the MUNC18-1 protein (Fig. 1E, top) in the hydrophobic core (Fig. 1E, bottom), and has not been documented before as either disease-causing or asymptomatic variant. In close proximity to L446F, multiple heterozygous disease-associated and asymptomatic mutations (gnomAD v2.1 for Ensembl gene ID ENSG00000136854; Karczewski *et al.*, 2019) are reported (Fig. 1E).

The L-F mutation supports viability and does not have a profound effect on cellular protein levels

Heterozygous *STXBP1* encephalopathy mutations have been reported to severely reduce Munc18-1 protein levels (Saitsu *et al.*, 2010; Guiberson *et al.*, 2018; Kovačević *et al.*, 2018). To assess the effect on protein levels, the L446F variant was expressed in HEK293 cells with wild-type or the previously characterized heterozygous disease mutation C522R as controls (Fig. 2A and Supplementary Fig. 2A). Munc18^{C552R} levels were 90% reduced, as reported previously (Kovačević *et al.*, 2018). Munc18^{L446F} levels showed a clear trend towards a reduction (not significant), albeit less severe than for Munc18^{C552R}. Power analysis predicted that 10 independent samples would be required to detect a 50% reduction at $P = 0.05$.

Munc18-1 serves an essential, cell-autonomous role in neuronal viability (Santos *et al.*, 2016). We tested whether the L446F mutation compromises this role by expressing Munc18^{WT}, Munc18^{L446F} or Munc18^{C522R} in Munc18-1 null mouse neurons. Neurons depending on Munc18^{L446F} or Munc18^{C522R} only, showed normal survival until 15 DIV. At DIV13–15, C522R levels were significantly lower than wild-type, whereas L446F levels again showed a trend towards reduced levels (not significantly different from wild-type and C522R) (Fig. 2B and Supplementary Fig. 2B). Power analysis predicted that 13 independent samples would be required to detect a 50% reduction at $P = 0.05$. Together, these data show that Munc18^{L446F} supports neuronal viability as well as wild-type Munc18-1 and has a less drastic effect on cellular protein levels than previously characterized heterozygous disease variants.

Neuronal morphology was analysed in single isolated Munc18-1 null neurons expressing Munc18^{WT} or Munc18^{L446F} (Fig. 2C). Dendrites of neurons expressing Munc18^{L446F} were 25% shorter than wild-type neurons (Fig. 2D) and the number of synapses per µm^2 dendrite was 15% lower (Fig. 2E). Munc18^{L446F} and Munc18^{WT} expressing neurons had similar synapse sizes (Fig. 2F) and

Table 1 Clinical features of affected sisters and direct relatives

Subject	1	2	3	4	5
Current age, years	51	23	26	28	20
Age at epilepsy onset, years	–	2	3	–	–
Duration of epilepsy, years	–	21	23	–	–
Previous febrile seizures	–	Yes (18 months)	No	–	–
Type of seizures	–	Tonic, tonic-clonic, atypical absences, atonic seizures, episodes of non-convulsive status	Tonic, tonic-clonic, atypical absences, atonic seizures, episodes of non-convulsive status	–	–
EEG	Normal	1.5–2 Hz generalized spike-and-wave; generalized fast rhythms at 12 Hz during sleep	1.5–2 Hz generalized spike-and-wave, generalized fast rhythms at 12 Hz during sleep	Normal	Normal
Brain MRI	Normal	Some subcortical areas of increased T_2-weighted signal intensity with no mass effect or contrast enhancement	Arnold-Chiari type 1 without syringomelia	NA	NA
Neurological exam	Normal	Kinetic and postural tremor of the arms and brisk reflexes	Kinetic and postural tremor of the arms, pes cavus	Normal	Normal
Neuropsychiatric symptoms	None	Severe mental retardation (IQ <35); moderate/severe behavioural problems with hyperactivity and aggressive behaviour	Moderate mental retardation (IQ 46); mild behavioural problems with hyperactivity and aggressive behaviour	None	None
Therapy	None	Valproate + felbamate + acetazolamide + levetiracetam + rufinamide	Valproate + levetiracetam + rufinamide + clobazam (partial seizure control)	None	None

The proband is a 23-year-old female, presenting with refractory epilepsy, severe intellectual disability (IQ <35), hyperactivity and aggressive behaviour. She showed developmental delay from birth and suffered from isolated febrile seizures at the age of 18 months. Tonic seizures during sleep were observed since the age of two. Afterwards, multiple seizure types occurred such as tonic, atypical absences, and 'drop attacks'. Awake and sleep EEG recordings revealed a slow and disorganized background activity, and the classic high voltage, generalized 1.5–2 Hz spike and wave activity in addition to bursts of 10–12 Hz generalized paroxysmal fast activity during slow sleep. Moreover, she also occasionally experienced catamenial non-convulsive status epilepticus which could last up to several hours. A 3 T brain MRI study revealed non-specific subcortical areas of increased T_2-weighted signal intensity. Several anti-seizure drugs were unsuccessful. She is currently on valproate, felbamate, acetazolamide, levetiracetam, and rufinamide. Her 26-year-old sister showed developmental delay and the same neurological phenotype featuring early-onset tonic, atypical absences, and 'drop attacks' from the age of 3 years, moderate intellectual disability (IQ = 46), hyperactivity and aggressive behaviour. Her EEG showed high-voltage, generalized 1.5–2 Hz spike and wave activity associated with bursts of generalized paroxysmal fast activity during slow sleep. A polytherapy with valproate, levetiracetam, rufinamide, and clobazam achieved a partial seizure control, with persistence of atypical absences and drop attacks, mainly during her menstrual cycle. A 3 T MRI study revealed Arnold-Chiari 1 malformation without syringomyelia. Their 51-year-old mother, and their 28- and 20-year-old sisters were asymptomatic and showed normal intelligence. NA = not available.

Munc18-1 levels in synapses and dendrites (Fig. 2G and H). Hence, neurons that depend on $Munc18^{L446F}$ have slightly reduced size and synapse density.

$Munc18^{L446F}$ enhances evoked synaptic transmission and reduced paired-pulse facilitation

Patch-clamp electrophysiology was used to compare synaptic transmission in Munc18-1 null mutant neurons expressing either $Munc18^{WT}$ or $Munc18^{L446F}$. The frequency of spontaneous miniature excitatory postsynaptic current (mEPSC) events (Fig. 3A and B) and their amplitude was similar between $Munc18^{WT}$ and $Munc18^{L446F}$ (Fig. 3C). However, the postsynaptic current in response to action potential stimulation (EPSC; Fig. 3D) was approximately 2-fold larger in neurons expressing $Munc18^{L446F}$ both in amplitude (Fig. 3E) and charge transferred during the response (Fig. 3F). The ratio between paired sets of stimuli (paired-pulse ratio, typical example shown in Fig. 3G) was significantly smaller for $Munc18^{L446F}$-expressing neurons at most time intervals (Fig. 3H).

In addition to single stimulation, we tested evoked synaptic responses to repetitive ('train') stimulation. The increased response to stimulation could be due to an increase in the number of vesicles that are release-ready, which can be estimated based on a pool-depleting stimulation train at 40 Hz frequency. The estimated size of the RRP (estimated by back-extrapolation, see Supplementary Fig. 3A) was similar in $Munc18^{WT}$ and $Munc18^{L446F}$ expressing neurons (Fig. 3I) and no difference was observed in the total charge transferred during a pool-depleting 40 Hz stimulation (Fig. 3J).

The difference in response amplitude observed upon single stimuli (Fig. 3E and F) was again observed at the start of the train stimulations at 10 and 40 Hz. The run-down of successive responses followed a similar kinetic pattern between $Munc18^{WT}$ and $Munc18^{L446F}$ expressing neurons (Fig. 3K and L for 10 and 40 Hz, respectively). The EPSC response to a single stimulation after high-frequency stimulation, termed 'recovery', was impaired in neurons expressing $Munc18^{L446F}$ up to 60 s after a high-frequency stimulation (Fig. 3M and N for 10 and 40 Hz, respectively). The EPSC amplitude of $Munc18^{L446F}$ neurons reached similar levels to $Munc18^{WT}$ but not the increased

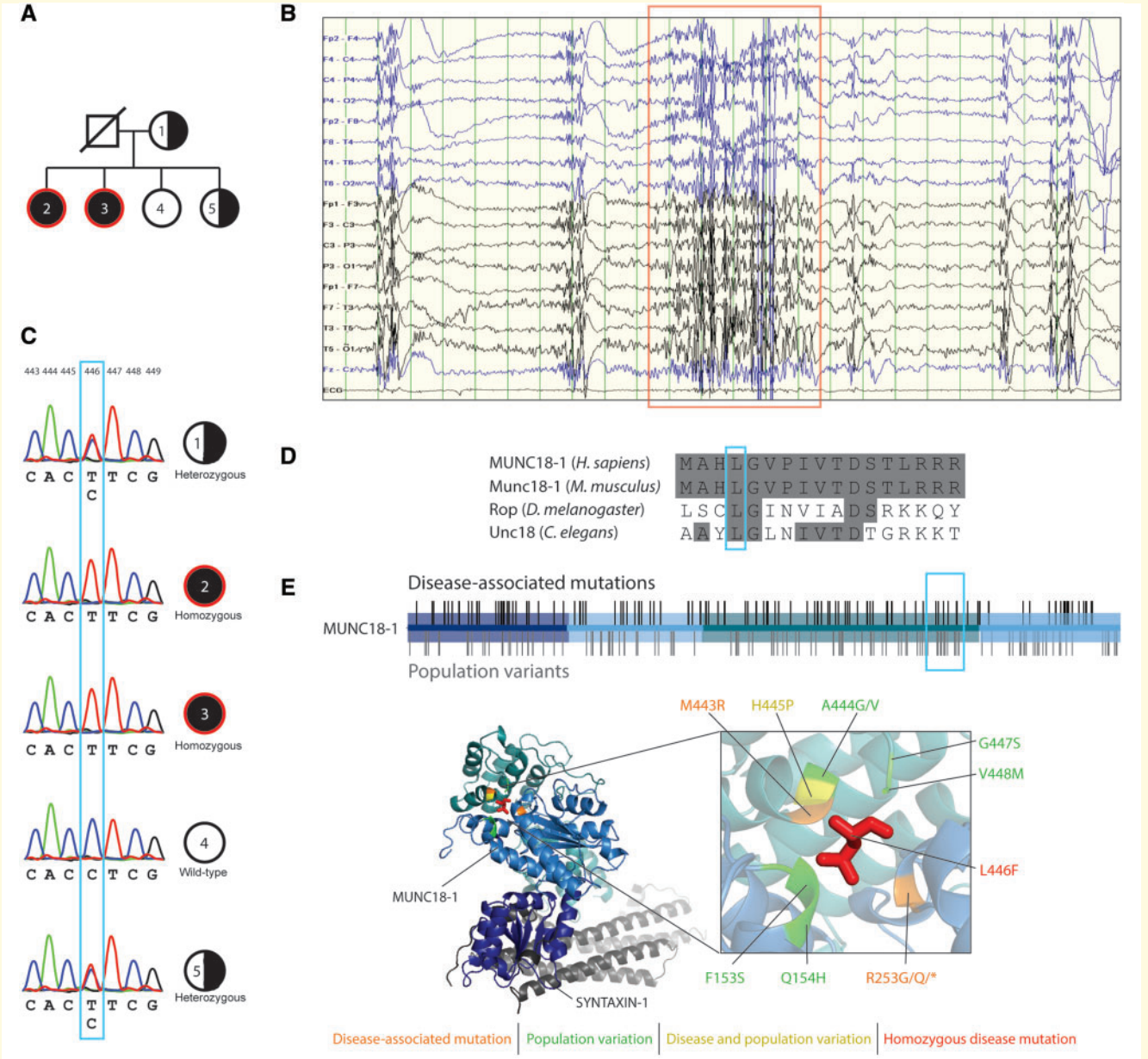

Figure 1 Identification of homozygous missense mutation MUNC18^{L446F} in two affected patients. (**A**) Pedigree of the family showing the two affected (red circle) homozygous sisters (dark filled circle) for the L446F missense mutation. One sibling does not carry the mutation and another one is heterozygous, as is the mother (half-filled circle). The father was not available for analysis. (**B**) EEG recording from one of the two homozygous carriers. Note the bursts of generalized paroxysmal fast activity at 10–12 Hz that last for a few seconds (red box) and tend to recur at brief intervals during slow sleep. The discharges are usually followed by slow waves and generalized poly-spike and wave complexes. (**C**) Electropherograms of the individuals as indicated in **A**, showing the c.1336 C > T missense mutation in Individuals 1 and 5 (heterozygous), 2 and 3 (homozygous). (**D**) Amino acid alignment of human MUNC18-1 protein to its homologues in *Mus musculus* (Munc18-1), *Drosophila melanogaster* (Rop) and *C. elegans* (Unc18). Blue box indicates the Leu446 residue, which is conserved across the indicated species. (**E**) Disease-associated mutations (black bars) and population variants (grey bars) are found throughout the three domains of the Munc18-1 protein. Leu446 is located in domain 3. Protein crystal structure of the Munc18-1 protein (PDB 3c98) bound to syntaxin 1 (grey) shows the Leu446 residue in red. Nearby disease-associated and population variants are indicated.

amplitude that was observed in naïve neurons (*cf.* Supplementary Fig. 3C and E).

The impaired recovery may be caused by a deficit in the recruitment of new synaptic vesicles into the RRP. However, the steady state vesicle recruitment, which can be estimated from the cumulative plots in Supplementary Fig. 3A, was not different between Munc18^{WT} or Munc18^{L446F} expressing neurons (Fig. 3O).

During repetitive stimulation, many vesicles fuse without tight coupling to the action potentials because of the build-

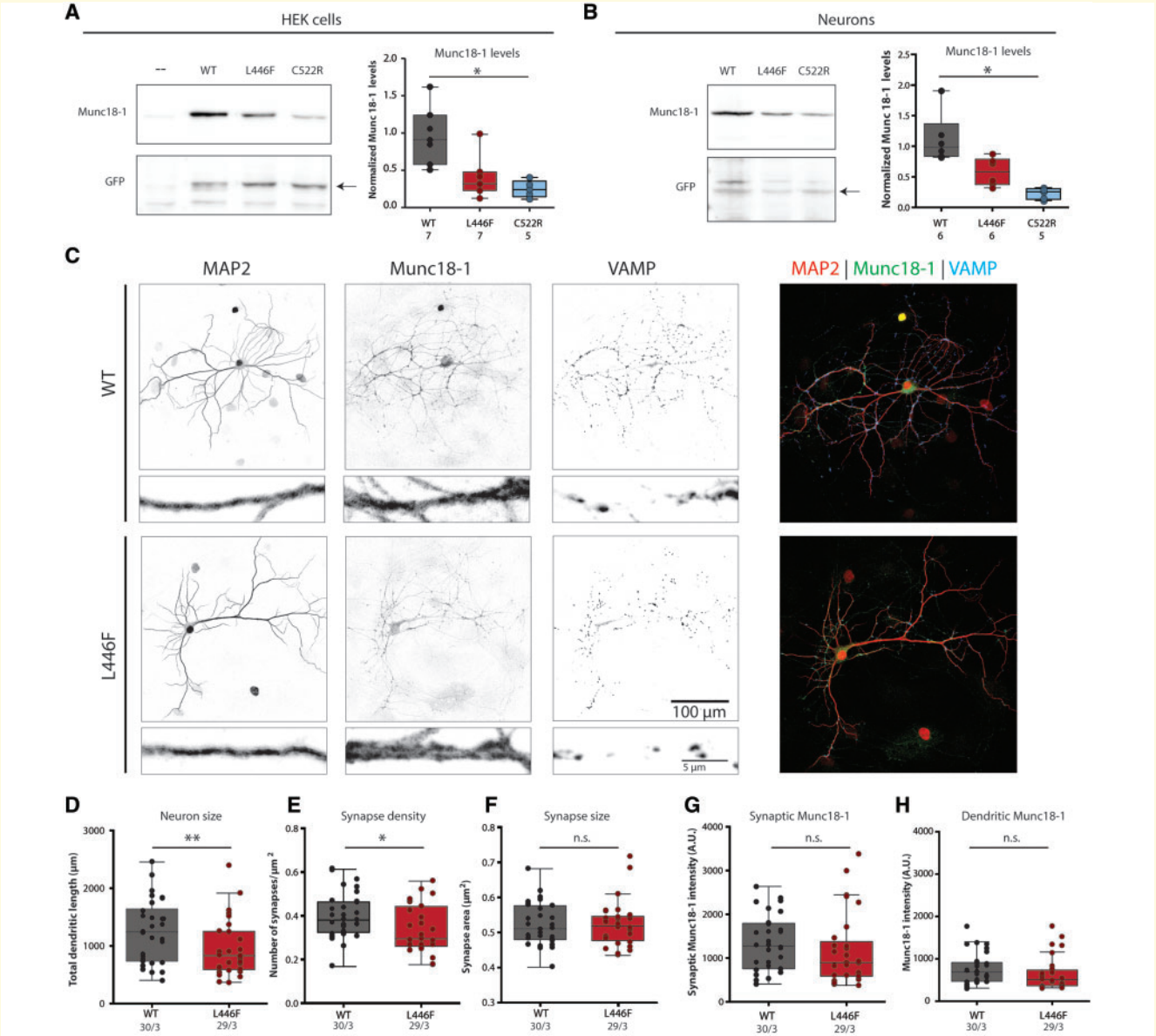

Figure 2 Cellular stability and morphological characterization of Munc18^{L446F} in Munc18-1 null neurons and HEK293 cells. (**A**) HEK293 cells were virally infected with Munc18^{WT}, homozygous pathogenic variant Munc18^{L446F} and heterozygous disease variant Munc18^{C522R}. Western blot analysis of normalized Munc18-1 levels shows that Munc18^{C522R} presents significantly lower levels than Munc18^{WT} [Munc18^{WT} median = 0.508, interquartile range (IQR) = 0.340–0.727; Munc18^{L446F} median = 0.187, IQR = 0.134–0.267; Munc18^{C522R} median = 0.143, IQR = 0.085–0.199; $P = 0.0006$, Kruskal-Wallis test with *post hoc* Dunn's multiple comparisons test]. Munc18^{L446F} has no significant changes in levels compared to either Munc18^{WT} and disease variant Munc18^{C522R}. Munc18 levels were normalized to GFP levels. Relative Munc18 levels were normalized to the mean Munc18^{WT} levels for visualization. (**B**) Munc18^{WT}, homozygous disease variant Munc18^{L446F} and heterozygous disease variant Munc18^{C522R} were expressed in Munc18-1 null neurons through lentiviral infection. Protein levels of Munc18^{C522R} are lower than Munc18^{WT} (Munc18^{WT} median = 1.587, IQR = 1.401–2.278; Munc18^{L446F} median = 0.978, IQR = 0.578–1.296; Munc18^{C522R} median = 0.397, IQR = 0.228–0.526; $P = 0.0012$, Kruskal-Wallis test with *post hoc* Dunn's multiple comparisons test), whereas levels of Munc18^{L446F} are not significantly different from Munc18^{WT} and Munc18^{C522R}. Munc18 levels were normalized to GFP levels. Relative Munc18 levels were normalized to the mean Munc18^{WT} levels for visualization. (**C**) Representative images (with zoom) of Munc18-1 null neurons expressing Munc18^{WT} or Munc18^{L446F}, stained for MAP2 (dendritic marker), Munc18-1 and VAMP (synaptic marker). (**D**) Total dendritic length is decreased in Munc18^{L446F} neurons (Munc18^{WT} median = 1243, IQR = 738–1645; Munc18^{L446F} median = 833.4, IQR = 592.5–1254; $P = 0.035$, Mann-Whitney U-test). (**E**) Munc18^{L446F} neurons show decreased number of synapses per µm^2 dendrite (Munc18^{WT} median = 0.382, IQR = 0.326–0.465; Munc18^{L446F} median = 0.296, IQR = 0.262–0.444; $P = 0.028$, unpaired *t*-test). (**F**) Average synapse area is not altered between neurons expressing Munc18^{WT} or Munc18^{L446F} (Munc18^{WT} median = 0.511, IQR = 0.480–0.577; Munc18^{L446F} median = 0.519, IQR = 0.477–0.547; $P = 0.894$, Mann-Whitney U-test). (**G** and **H**) Munc18^{L446F} neurons do not present lower Munc18-1 levels in synapses (**G**) (Munc18^{WT} median = 1276, IQR = 754.1–1789; Munc18^{L446F} median = 893.8, IQR = 584–1376; $P = 0.091$, Mann-Whitney U-test) or in dendrites (**H**) (Munc18^{WT} median = 654.6, IQR = 471–894; Munc18^{L446F} median = 479.7, IQR = 353.6–641.7; $P = 0.094$, Mann-Whitney U-test) by immunocytochemistry. The number of analysed cells and number of independent cultures tested is indicated below the graphs. $^{*}P < 0.05$, $^{**}P < 0.01$.

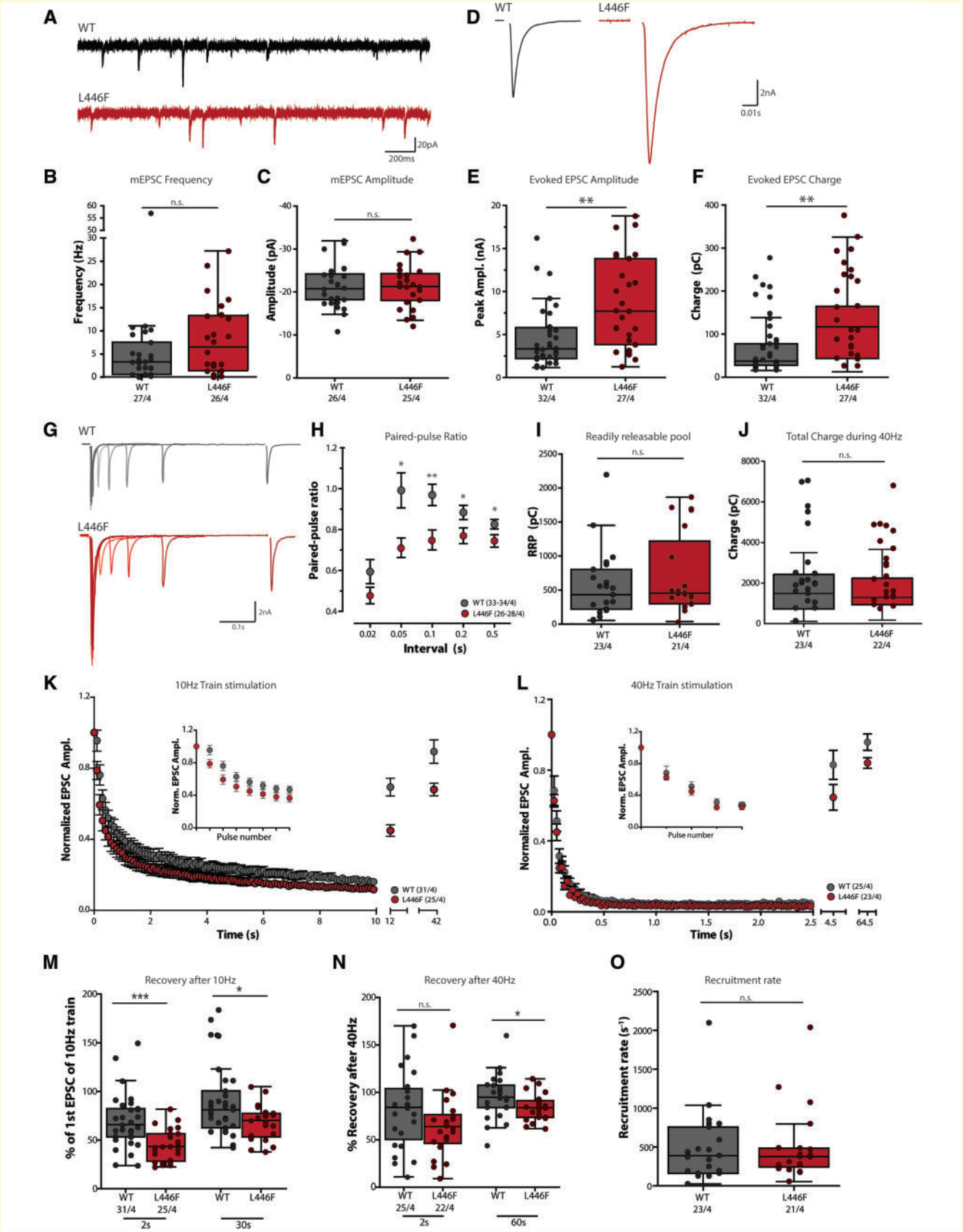

Figure 3 Patch-clamp electrophysiological characterization of Munc18-1 null neurons expressing Munc18^{L446F}. (**A**–**C**) Spontaneous release of synaptic vesicles is not significantly altered by expression of Munc18^{L446F}. (**A**) Example traces of spontaneous release of single synaptic vesicles (mEPSCs) of Munc18-1 null neurons expressing Munc18^{WT} or Munc18^{L446F}. (**B** and **C**) No differences are observed in

(continued)

up of Ca^{2+} in the terminals and possibly mediated by distinct release machinery ('asynchronous' release; for a review see Kaeser and Regehr, 2014). The relative contribution of synchronous and asynchronous components to the total charge transferred during the 40-Hz train was similar (Supplementary Fig. 3B). Together these data show that Munc18^{L446F} causes an increase in evoked synaptic transmission, a decrease in paired pulse plasticity and an impaired recovery following high-frequency stimulation.

Discussion

The present study identified two sisters carrying a homozygous *STXBP1* mutation. Functional analysis demonstrated that L446F mutation results in a gain-of-function at the cellular level unlike heterozygous mutations so far described (Guiberson *et al.*, 2018; Kovačević *et al.*, 2018).

The L446F mutation in *STXBP1*/ Munc18-1 causes a gain-of-function on synaptic transmission

Neurons expressing Munc18-1^{L446F} show a 2-fold increased synaptic response, indicating that twice as many synaptic vesicles fuse with the plasma membrane upon a single action potential stimulation than in neurons expressing wild-type Munc18-1. In addition, the paired-pulse ratio is reduced. This ratio is inversely proportional to the initial release probability of synaptic vesicles: a neuron with a high initial release probability releases a larger fraction of release-ready vesicles, and fewer remain for subsequent stimuli. Hence, these findings imply that Munc18^{L446F} causes a gain-of-function on evoked synaptic transmission by increasing the initial release probability. The L446F mutation may increase the release probability of vesicles indirectly, possibly by influencing 'superpriming' (Taschenberger *et al.*, 2016) of a larger fraction of synaptic vesicles and/or

Figure 3 Continued
spontaneous mEPSC frequency (**B**: Munc18^{WT} median = 3.253 Hz, IQR = 0.584–7.49; Munc18^{L446F} median = 6.473 Hz, IQR = 1.375–13.25; $P = 0.165$, Mann-Whitney U-test) and amplitude (**C**: Munc18^{WT} median = –20.76 pA, IQR = –24.19–18.24; Munc18^{L446F} median = –21.28 pA, IQR = –24.29–18.03; $P = 0.943$, unpaired *t*-test) between Munc18^{WT} and Munc18^{L446F}. (**D**–**F**) Evoked synaptic responses are increased in neurons expressing Munc18^{L446F}. (**D**) Typical examples of a single evoked EPSC. Stimulus artefact has been blanked out for visualization purposes. (**E**) Average EPSC amplitude is significantly larger in neurons expressing Munc18^{L446F} compared Munc18^{WT} (Munc18^{WT} median = 3.332 nA, IQR = 2.213–5.798; Munc18^{L446F} median = 7.716 nA, IQR = 3.838–13.81; $P = 0.0018$, Mann-Whitney U-test) and in parallel, the average charge (**F**) transferred during the EPSC response is increased (Munc18^{WT} median = 37.36 pC, IQR = 27.65–77.65; Munc18^{L446F} median = 117.0 pC, IQR = 43.69–164.7; $P = 0.0012$, Mann-Whitney U-test). (**G** and **H**) Paired-pulse recordings at various intervals were performed to quantify release probability. (**G**) Example traces showing an overlay of paired-pulse recordings at several time intervals (20–50–100–200–500 ms interpulse interval) for a neuron expressing Munc18^{WT} or Munc18^{L446F}. (**H**) Paired-pulse ratios (calculated as the ratio of the second EPSC to the first EPSC) are significantly higher for neurons expressing Munc18^{L446F} at the stimulus intervals between 0.05 and 0.5 s (0.02 s: Munc18^{WT} median = 0.488, IQR = 0.363–0.880; Munc18^{L446F} median = 0.479, IQR = 0.317–0.657, $P = 0.109$, unpaired *t*-test with Welch's correction; 0.05 s: Munc18^{WT} median = 0.872, IQR = 0.689–1.198; Munc18^{L446F} median = 0.701, IQR = 0.544–0.849, $P = 0.0103$; 0.1 s: Munc18^{WT} median = 0.913, IQR = 0.743–1.157; Munc18^{L446F} median = 0.732, IQR = 0.589–0.891, $P = 0.0045$; 0.2 s: Munc18^{WT} median = 0.873, IQR = 0.754–0.955, Munc18^{L446F} median = 0.777, IQR = 0.625–0.866, $P = 0.0207$; 0.5 s: Munc18^{WT} median = 0.833, IQR = 0.775–0.905, Munc18^{L446F} median = 0.751, IQR = 0.614–0.839, $P = 0.019$, Mann-Whitney U-tests). (**I**) Estimate of the RRP by back-extrapolation indicates no difference in RRP size between Munc18^{WT} or Munc18^{L446F} (Munc18^{WT} median = 432.7 pC, IQR = 220.1–803.6, Munc18^{L446F} median = 455.4 pC, IQR = 300.3–1219, $P = 0.511$, Mann-Whitney U-test). (**J**) Total charge transferred during the 40-Hz train stimulation is not significantly different between Munc18^{WT} or Munc18^{L446F} (Munc18^{WT} median = 1488 pC, IQR = 724.4–2424, Munc18^{L446F} median = 1296 pC, IQR = 939.0–2239, $P = 0.594$, Mann-Whitney U-test). (**K**) Run-down kinetics and steady-state responses to 100 action potentials at 10 Hz are similar between Munc18^{WT} and Munc18^{L446F}, except for the first few pulses (*inset*) at which neurons expressing Munc18^{L446F} display more pronounced depression compared to Munc18^{WT}. (**L**) EPSC rundown in response to a stimulation of 100 action potentials at 40 Hz are also similar between Munc18^{WT} and Munc18^{L446F}. *Inset*: first five pulses of the train. (**M**) EPSC amplitude in response to single action potential stimulations 2 and 30 s after the 10-Hz train stimulation expressed as a percentage of the amplitude of the first EPSC of the train stimulation. Neurons expressing Munc18^{L446F} have a smaller EPSC response at 2 s (Munc18^{WT} median = 65.96%, IQR = 53.26–82.32, Munc18^{L446F} median = 43.27%, IQR = 28.32–56.44, $P = 0.0003$, Mann-Whitney U-test) and 30 s (Munc18^{WT} median = 81.15%, IQR = 62.58–100.6, Munc18^{L446F} median = 70.29%, IQR = 53.31–77.36, $P = 0.021$, Mann-Whitney U-test) after a 10-Hz train. (**N**) Recovery of the RRP was measured at 2 and 60 s after the train, respectively. After 2 s, recovery is not significantly different but shows a trend towards a reduction in Munc18^{L446F} expressing neurons (Munc18^{WT} median = 84.22%, IQR = 50.45–104.0, Munc18^{L446F} median = 63.92%, IQR = 46.39–76.59, $P = 0.068$, Mann-Whitney U-test). Sixty seconds after 40-Hz stimulation, neurons expressing Munc18^{WT} show full recovery whereas recovery is impaired in neurons expressing Munc18^{L446F} (Munc18^{WT} median = 94.90%, IQR = 83.97–107.5, Munc18^{L446F} median = 83.93%, IQR = 73.73–91.31, $P = 0.0396$, unpaired *t*-test with Welch's correction). (**O**) Recruitment rate of vesicles at steady-state during 40 Hz stimulation as estimated by the back-extrapolation procedure (**C**) is not different between Munc18^{WT} or Munc18^{L446F} (Munc18^{WT} median = 388.5 s^{-1}, IQR = 160.7–755.8, Munc18^{L446F} median = 377.3 s^{-1}, IQR = 243.4–484.4, $P = 0.778$, Mann-Whitney U-test). The number of analysed cells and number of independent cultures tested is indicated below the graphs. $^{*}P < 0.05$, $^{**}P < 0.01$.

by more efficiently preventing the off-pathway (de-priming) (He *et al.*, 2017; Prinslow *et al.*, 2019).

A gain-of-function phenotype in synaptic genetic disorders is rare, as disease-associated mutations in presynaptic genes are typically loss-of-function (Fassio *et al.*, 2011; Corradini *et al.*, 2014; Schubert *et al.*, 2014; Baker *et al.*, 2015). However, a gain-of-function phenotype was recently observed for the presynaptic protein Munc13, also resulting in a severe neurodevelopmental disorder (Lipstein *et al.*, 2017).

Homozygous *STXBP1*-variant L446F causes specific symptoms of Lennox-Gastaut syndrome

STXBP1-encephalopathy cases share two to three main clinical features (developmental delay, intellectual disability, and almost always epilepsy), but individual patients show substantial clinical heterogeneity and the primary diagnosis is diverse, including Ohtahara and West syndromes (Stamberger *et al.*, 2016). To date, only two heterozygous *STXBP1* carriers have been diagnosed as Lennox-Gastaut syndrome based on minimal (Epi4K Consortium *et al.*, 2013) or undisclosed (Carvill *et al.*, 2013) criteria. For homozygous L446F carriers described in the current study, the electroclinical phenotype is clearly pathognomonic for Lennox-Gastaut syndrome (Cross *et al.*, 2017): (i) multiple seizure types, including tonic, atonic and atypical absence seizures, with predominantly nocturnal tonic seizures; (ii) abnormal EEG, with interictal, diffuse, slow spike-wave complexes at <3 Hz during wakefulness; and (iii) paroxysmal fast rhythms (10–20 Hz) during non-REM sleep. These features may eventually emerge in more than the two heterozygous patients described to date as a progressive aspect of STXBP1 encephalopathy. However, none of the other >250 heterozygous carriers characterized to date (Fig. 1E), have had these three cardinal pathognomonic Lennox-Gastaut syndrome criteria described. Hence, the combination of these three Lennox-Gastaut syndrome symptoms may be unique for the (homozygous) L446F variant, for gain-of-function *STXBP1* mutations and/or for recessive mutations. Exome sequencing did not reveal additional variants that could be readily associated to the phenotype, but we cannot exclude that the other genetic factors may contribute to the clinical profile.

Loss- and gain-of-function *STXBP1* mutations cause shared and unique clinical features

Heterozygous *STXBP1* encephalopathy mutations are clear loss-of-function mutations in terms of protein stability and some also of synaptic transmission (Guiberson *et al.*, 2018; Kovačević *et al.*, 2018). In contrast, the Munc18^{L446F} mutation has a less pronounced effect on protein stability, and a gain-of-function effect on synaptic transmission. Thus, at the synaptic level, homozygous and heterozygous disease mutations have opposite effects. At the clinical level, the two homozygous patients display all three main clinical *STXBP1* encephalopathy features (developmental delay, intellectual disability, epilepsy). Hence, opposite effects at the synaptic level lead to the same main clinical features. Different (opposite) changes in the molecular function of MUNC18-1 may ultimately lead to a similar net activity imbalance at the brain circuit level and thereby to the same clinical features. However, at the phenotypic level, the L446F homozygous mutation leads to distinct (electroclinical) symptoms, characteristic of Lennox-Gastaut syndrome. These distinct symptoms may provide the first indications of underlying heterogeneity between homozygous and heterozygous disease mutations and/or between gain- and loss-of-function mutations. More detailed clinical assessments, especially of seizure types and EEG abnormalities, will be instrumental for future subclassification of *STXBP1* cases, to unmask differential disease mechanisms at the network level and to design rational intervention strategies.

Previous studies have shown that both loss- and gain-of-function heterozygous mutations produce similar epileptic encephalopathies, e.g. for mutations in *KCNA2*, *SCN2A* and *SCNA8* (Larsen *et al.*, 2015; Masnada *et al.*, 2017; Wolff *et al.*, 2017). Recently, two homozygous cases carrying *SCN2A* mutations have been reported to lead to severe complex neurological phenotypes (AlSaif *et al.*, 2019; Yılmaz, 2019). These findings are consistent with other neurological dominant disorders, where very rare homozygous individuals share a similar phenotype with heterozygous family members, usually more severe, suggesting an additive effect on the gene product dysfunction (Wexler *et al.*, 1987; Labate *et al.*, 2012). However, functional analysis was not available for these variants. The situation for *STXBP1* mutations seems to be quite unique, displaying the same main clinical features for carriers of homozygous mutations that are recessive and of heterozygous mutations that cause haploinsufficiency. Thus, our study highlights the impact of allelic diversity and specificity in the pathogenesis and phenotypic expression of monogenic neurological disorders.

Acknowledgements

The authors thank Robbert Zalm for his help with cloning and virus production, Joke Wortel for breeding mutant mice and Joost Hoetjes genotyping of mutant mice. We thank Ingrid Saarloos for culturing of HEK293 cells, and Frank den Oudsten and Desiree Schut for preparation of glia feeder plates. The authors also thank Vincent Huson for developing MATLAB routines used for analysis of the electrophysiological data.

Funding

This work was supported by the Italian League against Epilepsy (F.Z.), the Italian Ministry of Health (RF-2016-

02361949, F.Z.); Era-Net Neuron (SNAREopathy to F.Z.), R.F.T. was supported by the Netherlands Scientific Organisation and De Hersenstichting (013-17-002), under the frame of Neuron Cofund ERA-Net SNAREopathy; COSYN (Comorbidity and Synapse Biology in Clinically Overlapping Psychiatric Disorders; Horizon 2020 Program of the European Union under RIA grant agreement 667301 to M.V.); a European Research Council (ERC) advanced grant (322966) of the European Union (to M.V.).

Competing interests

The authors report no competing interests.

Supplementary material

Supplementary material is available at *Brain* online.

References

AlSaif S, Umair M, Alfadhel M. Biallelic *SCN2A* gene mutation causing early infantile epileptic encephalopathy: case report and review. J Cent Nerv Syst Dis 2019; 11: 117957351984993.

Baker K, Gordon SL, Grozeva D, van Kogelenberg M, Roberts NY, Pike M, et al. Identification of a human synaptotagmin-1 mutation that perturbs synaptic vesicle cycling. J Clin Invest 2015; 125: 1670–8.

Carvill GL, Heavin SB, Yendle SC, McMahon JM, O'Roak BJ, Cook J, et al. Targeted resequencing in epileptic encephalopathies identifies de novo mutations in CHD2 and SYNGAP1. Nat Genet 2013; 45: 825–30.

Cijsouw T, Weber JP, Broeke JH, Broek JAC, Schut D, Kroon T, et al. Munc18-1 redistributes in nerve terminals in an activity- and PKC-dependent manner. J Cell Biol 2014; 204: 759–75.

Corradini I, Donzelli A, Antonucci F, Welzl H, Loos M, Martucci R, et al. epileptiform activity and cognitive deficits in SNAP-25 +/– mice are normalized by antiepileptic drugs. Cereb Cortex 2014; 24: 364–76.

Cross JH, Auvin S, Falip M, Striano P, Arzimanoglou A. Expert opinion on the management of Lennox–Gastaut Syndrome: treatment algorithms and practical considerations. Front Neurol 2017; 8: 505.

Epi4K Consortium; Allen AS, Berkovic SF, Cossette P, Delanty N, Dlugos D, et al. De novo mutations in epileptic encephalopathies. Nature 2013; 501: 217–21.

Fassio A, Patry L, Congia S, Onofri F, Piton A, Gauthier J, et al. SYN1 loss-of-function mutations in autism and partial epilepsy cause impaired synaptic function. Hum Mol Genet 2011; 20: 2297–307.

Gburek-Augustat J, Beck-Woedl S, Tzschach A, Bauer P, Schoening M, Riess A. Epilepsy is not a mandatory feature of STXBP1 associated ataxia-tremor-retardation syndrome. Eur J Paediatr Neurol 2016; 20: 661–5.

Guiberson NGL, Pineda A, Abramov D, Kharel P, Carnazza KE, Wragg RT, et al. Mechanism-based rescue of Munc18-1 dysfunction in varied encephalopathies by chemical chaperones. Nat Commun 2018; 9: 3986.

Hamdan FF, Gauthier J, Dobrzeniecka S, Lortie A, Mottron L, Vanasse M, et al. Intellectual disability without epilepsy associated with STXBP1 disruption. Eur J Hum Genet 2011; 19: 607–9.

He E, Wierda K, van Westen R, Broeke JH, Toonen RF, Cornelisse LN, et al. Munc13-1 and Munc18-1 together prevent NSF-dependent de-priming of synaptic vesicles. Nat Commun 2017; 8: 15915.

Kaeser PS, Regehr WG. Molecular mechanisms for synchronous, asynchronous, and spontaneous neurotransmitter release. Annu Rev Physiol 2014; 76: 333–63.

Karczewski KJ, Francioli LC, Tiao G, Cummings BB, Alföldi J, Wang Q, et al. Variation across 141, 456 human exomes and genomes reveals the spectrum of loss-of-function intolerance across human protein-coding genes. bioRxiv 2019; 531210.

Kovačević J, Maroteaux G, Schut D, Loos M, Dubey M, Pitsch J, et al. Protein instability, haploinsufficiency, and cortical hyperexcitability underlie STXBP1 encephalopathy. Brain 2018; 141: 1350–74.

Labate A, Tarantino P, Viri M, Mumoli L, Gagliardi M, Romeo A, et al. Homozygous c.649dupC mutation in *PRRT2* worsens the BFIS/PKD phenotype with mental retardation, episodic ataxia, and absences. Epilepsia 2012; 53: e196–9.

Larsen J, Carvill GL, Gardella E, Kluger G, Schmiedel G, Barisic N, et al. The phenotypic spectrum of SCN8A encephalopathy. Neurology 2015; 84: 480–9.

Lipstein N, Verhoeven-Duif NM, Michelassi FE, Calloway N, Van Hasselt PM, Pienkowska K, et al. Synaptic UNC13A protein variant causes increased neurotransmission and dyskinetic movement disorder. J Clin Invest 2017; 127: 1005–18.

Masnada S, Hedrich UBS, Gardella E, Schubert J, Kaiwar C, Klee EW, et al. Clinical spectrum and genotype–phenotype associations of KCNA2-related encephalopathies. Brain 2017; 140: 2337–54.

Meijer M, Cijsouw T, Toonen RF, Verhage M. Synaptic effects of Munc18-1 alternative splicing in excitatory hippocampal neurons. PLoS One 2015; 10: 1–14.

Naldini L, Blomer U, Gallay P, Ory D, Mulligan R, Gage F, et al. In vivo gene delivery and stable transduction of nondividing cells by a lentiviral vector. Science (80-) 1996; 272: 263–7.

Neher E. Merits and limitations of vesicle pool models in view of heterogeneous populations of synaptic vesicles. Neuron 2015; 87: 1131–42.

Orock A, Logan S, Deak F. Munc18-1 haploinsufficiency impairs learning and memory by reduced synaptic vesicular release in a model of Ohtahara syndrome. Mol Cell Neurosci 2018; 88: 33–42.

Prinslow EA, Stepien KP, Pan Y-Z, Xu J, Rizo J. Multiple factors maintain assembled trans-SNARE complexes in the presence of NSF and alpha-SNAP. Elife 2019.

Saitsu H, Kato M, Mizuguchi T, Hamada K, Osaka H, Tohyama J, et al. De novo mutations in the gene encoding STXBP1 (MUNC18-1) cause early infantile epileptic encephalopathy. Nat Genet 2008; 40: 782–8.

Saitsu H, Kato M, Okada I, Orii KE, Higuchi T, Hoshino H, et al. STXBP1 mutations in early infantile epileptic encephalopathy with suppression-burst pattern. Epilepsia 2010; 51: 2397–405.

Santos T, Wierda K, Broeke J, Toonen R, Verhage M. Early Golgi abnormalities and neurodegeneration upon loss of presynaptic proteins Munc18-1, Syntaxin-1, or SNAP-25. J Neurosci 2016; 37: 4525–39.

Schmitz SK, Hjorth JJJ, Joemai RMS, Wijntjes R, Eijgenraam S, de Bruijn P, et al. Automated analysis of neuronal morphology, synapse number and synaptic recruitment. J Neurosci Methods 2011; 195: 185–93.

Schubert J, Siekierska A, Langlois M, May P, Huneau C, Becker F, et al. Mutations in STX1B, encoding a presynaptic protein, cause fever-associated epilepsy syndromes. Nat Genet 2014; 46: 1327–32.

Stamberger H, Nikanorova M, Accorsi P, Angriman M, Benkel-herrenbrueck I, Capovilla G, et al. STXBP1 encephalopathy: a neurodevelopmental disorder including epilepsy. Neurology 2016; 1–10.

Taschenberger H, Woehler A, Neher E. Superpriming of synaptic vesicles as a common basis for intersynapse variability and modulation of synaptic strength. Proc Natl Acad Sci 2016; 113: E4548–E4557.

Toonen RFG, Verhage M. Munc18-1 in secretion: lonely Munc joins SNARE team and takes control. Trends Neurosci 2007; 30: 564–72.

Toonen RFG, Wierda K, Sons MS, Wit HD, Cornelisse LN, Brussaard A, et al. Munc18-1 expression levels control synapse recovery by regulating readily releasable pool size. Proc Natl Acad Sci 2006; 103: 1–6.

Verhage M, Maia AS, Plomp JJ, Brussaard AB, Heeroma JH, Vermeer H, et al. Synaptic assembly of the brain in the absence of neurotransmitter secretion. Science (80-) 2000; 287: 864–9.

Wexler NS, Young AB, Tanzi RE, Travers H, Starosta-Rubinstein S, Penney JB, et al. Homozygotes for Huntington's disease. Nature 1987; 326: 194–7.

Wolff M, Johannesen KM, Hedrich UBS, Masnada S, Rubboli G, Gardella E, et al. Genetic and phenotypic heterogeneity suggest therapeutic implications in SCN2A-related disorders. Brain 2017; 140: 1316–36.

Yılmaz HÖ. Homozygous SCN2A gene mutation causing early infantile epileptic encephalopathy: the second case in literature. Med Sci Discov 2019; 6: 221–3.